

Inversion of Love wave phase velocity, group velocity and shear stress ratio using finite elements

Matthew Haney (Boise State University) and Huub Douma* (ION Geophysical/GXT Imaging solutions)

SUMMARY

We present the theory of Love wave inversion for shear velocity profiles using phase velocity, group velocity, and shear stress ratio measurements. This theory can be used to setup practical inversion schemes to estimate the near-surface velocity structure in the Earth. The method is founded on the forward modeling method developed by Lysmer (1970) who used a finite-element method to model Rayleigh waves. The advantage of the employed method is that the depth-sensitivity functions needed to calculate the gradients follow from an eigenvalue problem, which can be solved in a fast manner using standard eigenvalue/eigenvector solvers.

INTRODUCTION

Surface waves are sensitive to the near-surface Earth structure and as such carry valuable information about this often complex zone. In global seismology, surface waves have for a long time been the dominant source of information to obtain the velocity structure in the Earth's crust (Dorman & Ewing, 1962; Aki & Richards, 2002). In exploration seismology, surface waves are mostly treated as noise as they mask the body-wave reflections used in seismic imaging. Recently surface waves have received more attention in exploration seismics in an attempt to use them to characterize near-surface structure [e.g., Xia *et al.* (1999), Ivanov *et al.* (2006), Muzert (2007) and Gouédard *et al.* (2010)], that can be complex in both land and ocean-bottom seismic surveys.

The forward modeling method of surface waves described in this work originates from Lysmer (1970), who used it for modeling of Rayleigh waves. The method is in principle a finite-element method but can be viewed as the simplest form of a spectral element (or continuous Galerkin) method (Patera, 1984; Komatitsch & Vilotte, 1998), as it uses a linear interpolation across the elements. It is different from conventional methods for modeling of surface waves in that it leads to a simple linear system of equations that can be solved with conventional numerical methods. Based on Lysmer's forward modeling formulation, here applied to Love waves instead of Rayleigh waves, the linear inverse problem formulation is found through a first-order perturbation analysis. Such an inversion based on Lysmer's method has previous been implemented for Rayleigh waves by Masterlark *et al.* (2010) in order to image a shallow magma chamber. We present the inverse problem for both group velocity and phase velocity measurements of Love waves.

In addition to phase and group velocities, the HZ ratio or ellipticity of Rayleigh waves can also be inverted for near-surface structure (Tanimoto & Tsuboi, 2009; Haney *et al.*, 2011). So far, no extension of this method has been proposed for Love waves. This makes sense because Love waves have only one direction of particle motion, in the out-of-plane direction. How-

ever, we find that the two shear stresses associated with the SH system are 90° out of phase just like the vertical and radial particle motions for Rayleigh waves. Therefore, if measurements of these stress components can be made, their ratio can be inverted for a shear wave velocity profile in a manner analogous to inversion of Rayleigh wave HZ ratio.

FORWARD MODELING

In an isotropic medium that varies only with depth, the wave equation for SH-waves is given by

$$\mu(\partial_x^2 u_y + \partial_z^2 u_y) + (\partial_z \mu)(\partial_z u_y) = \rho \partial_t^2 u_y, \quad (1)$$

where μ is the shear modulus, ρ the density and u_y the y-component of the displacement. We seek a weak-form solution by taking the inner product with a (non-zero) test function w . Therefore we have

$$\int_V [\rho \omega^2 u_y + \mu(\partial_x^2 u_y + \partial_z^2 u_y) + (\partial_z \mu)(\partial_z u_y)] w \, dV = 0, \quad (2)$$

where we transformed into the frequency domain using the temporal Fourier transform. Since the medium varies only with depth, we look for a solution of the form

$$u_y(x, z, t) = r(z) e^{i(kx - \omega t)}, \quad (3)$$

where k is the horizontal wavenumber and $r(z)$ describes the depth sensitivity of the solution. We seek a piecewise linear solution. Therefore we project the solution (as well as the test-function) onto the basis

$$\phi_i(z) = \begin{cases} (z - z_{i-1})/h_{i-1} & \text{if } z_{i-1} < z < z_i, \\ (z_{i+1} - z)/h_i & \text{if } z_i \leq z < z_{i+1}, \\ 0 & \text{otherwise.} \end{cases} \quad (4)$$

The model parameters μ and ρ are assumed to be piecewise constant; i.e., we assume a layered 1D model. The model parameters are therefore projected onto the basis

$$\Pi_i(z) = \begin{cases} 1 & \text{if } z_i \leq z < z_{i+1}, \\ 0 & \text{otherwise.} \end{cases} \quad (5)$$

Since in the horizontal direction we assume purely harmonic motion, the integral over the volume V can be replaced with an interval over depth. Consider one layer only with index n , i.e. $z_n < z < z_{n+1}$. Since for $z_n < z < z_{n+1}$ we have $\phi_j(z) \neq 0$ only if $j \in \{n, n+1\}$, we must have

$$\begin{aligned} & \int_{z_n}^{z_{n+1}} \omega^2 \left(\sum_{l=1}^N \rho_l \Pi_l \right) \left(\sum_{i=1}^N r_i \phi_i \phi_j \right) \\ & + \left(\sum_{l=1}^N \mu \Pi_l \right) \left(\sum_{i=1}^N r_i \partial_z^2 \phi_i \phi_j - k^2 \sum_{i=1}^N r_i \phi_i \phi_j \right) \\ & - \left(\sum_{l=1}^N \mu \Pi_l \right) \left(\sum_{i=1}^N r_i \partial_z [(\partial_z \phi_i) \phi_j] \right) \, dz \\ & + [\mu(\partial_z r) \phi_j]_{z_n}^{z_{n+1}} = 0, \end{aligned} \quad (6)$$

where $J \in \{n, n+1\}$, N is the total number of layers, and where r_i is the i -th coefficient of the projection of $r(z)$ onto basis ϕ , and where ρ_l and μ_l are the l -th coefficients of the projection of ρ and μ onto basis Π , respectively. The last term in equation 6 is the boundary term that results from integration by parts of the last term in equation 2. We shall first proceed to ignore the boundary terms and return to them at the end of this section.

Since for $z_n < z < z_{n+1}$ we have $\Pi_l(z) \neq 0$ only if $l = n$, the sums over l contribute only the term for $l = n$. The remaining terms then involve products $\Pi_n \phi_i$. These products are only nonzero if $i \in \{n, n+1\}$. Using this it follows from equation 6 that we have

$$\begin{aligned} & (\omega^2 \rho_n - k^2 \mu_n) \left[\sum_{i=n}^{n+1} r_i \int_{z_n}^{z_{n+1}} \phi_i \phi_J dz \right] \\ & + \mu_n \left[\sum_{i=n}^{n+1} r_i \int_{z_n}^{z_{n+1}} (\partial_z^2 \phi_i) \phi_J dz \right] \\ & - \mu_n \left[\sum_{i=n}^{n+1} r_i \int_{z_n}^{z_{n+1}} \partial_z [(\partial_z \phi_i) \phi_J] dz \right] = 0. \end{aligned} \quad (7)$$

Since here $J \in \{n, n+1\}$, we see that equation 7 is a linear system of two equations with two unknowns, i.e., r_n and r_{n+1} . The integrals involving the basis-functions ϕ can be evaluated using the definition of this basis in equation 4. By defining the vector $v := [r_n r_{n+1}]^T$, we can write equation 7 in matrix form as

$$\omega^2 M v = (k^2 B_2 + B_0) v, \quad (8)$$

with the matrices M , B_2 and B_0 given by

$$M := \rho_n h_n K, \quad B_2 := \mu_n h_n K, \quad B_0 := \frac{\mu_n}{h_n} L, \quad (9)$$

with

$$K := \begin{pmatrix} 1/3 & 1/6 \\ 1/6 & 1/3 \end{pmatrix}, \quad L := \begin{pmatrix} 1 & -1 \\ -1 & 1 \end{pmatrix}. \quad (10)$$

In equation 9 h_n denotes the thickness of layer n . The mass matrix M can be replaced with a diagonal matrix by "mass lumping", i.e., summing the entries in each row of M and placing the sum on the main diagonal. The matrices given in equation 9 were previously also given by Lysmer & Drake (1971).

Equation 8 holds for a single layer. The multi-layered-case matrices can be assembled from the elemental matrices in equation 9 by a process illustrated in figure 1. Knowing that we have ignored the boundary terms in equation 6, we mention that for internal boundaries the boundary terms of different layers cancel each other since we consider welded boundary conditions. The only boundary terms that remain are the external boundary terms, i.e., the upper boundary of the uppermost layer and the lower boundary of the lowermost layer. The boundary term at the upper interface vanishes since we assume a stress free surface and the term at the lower interface vanishes because there we implement a Dirichlet boundary condition (Lysmer, 1970). The Dirichlet boundary condition implies that the forward modeling uses the "locked-mode approximation" (Nolet *et al.*, 1989). In practice, this means that the model in depth must extend at least 1 wavelength in depth for accurate modeling (Lysmer, 1970). The additional requirement for accurate forward modeling is that the individual layers be at least

as thin as one-tenth of the wavelength. This requirement has led to the method being called the "thin-layer method" (Kausel & Roësset, 1981).

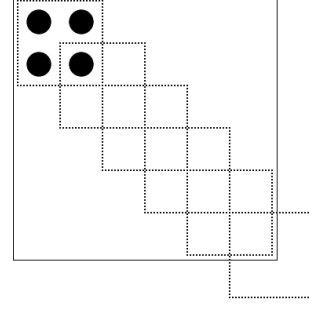


Figure 1: Illustration of assembly of elemental matrices for a single layer (small square) into matrices for full multi-layered model (big square). Remaining entries of the deepest elemental matrix are simply not used.

Equation 8 is a generalized eigenvalue problem with k^2 as eigenvalue and the depth-sensitivity coefficients v as eigenvectors. Solving this eigenvalue problem for a fixed frequency then provides the depth sensitivity functions $r(z)$ for the different modes. Since the fundamental mode has the lowest phase velocity, it corresponds to the largest eigenvalue. Once the depth sensitivity functions $r(z)$ are found for the different modes, equation 3 can be used to model wave-propagation for a given depth model by summing over all modes, or, if only certain modes are desired, by considering different modes separately.

GROUP VELOCITY

The group velocity u of surface waves is given by

$$u = \frac{\partial \omega}{\partial k}. \quad (11)$$

To find an expression for the group velocity we perturb ω , k and v in equation 8, while keeping the model parameters μ and ρ constant. Doing this while keeping only first order terms, and using that due to the symmetry of matrices M , B_2 and B_0 we have

$$\omega^2 v^T M = v^T (k^2 B_2 + B_0), \quad (12)$$

it follows that the group velocity can be written as

$$u = \frac{k}{\omega} \frac{v^T B_2 v}{v^T M v}. \quad (13)$$

PHASE-VELOCITY INVERSION

We first consider the phase velocity. To allow inversion of the phase velocity for the model parameters, we seek a linear relation between a perturbation in the phase-velocity and perturbations in the model parameters. Therefore, we perturb k , μ , ρ and v while keeping the frequency constant. Doing this while

keeping only first-order terms and again using equation 12 it follow that

$$2kdkv^T B_2 v = \omega^2 v^T \left(\sum_{i=1}^N \frac{\partial M}{\partial \rho_i} d\rho_i \right) v - v^T \left(\sum_{i=1}^N \frac{\partial (k^2 B_2 + B_0)}{\partial \mu_i} d\mu_i \right) v. \quad (14)$$

Using that for fixed frequency we have $dk/k = -dc/c$ with c the phase-velocity, it follows that equation 14 can be written as

$$\frac{dc}{c} = \left(K_\mu^c \Big|_\rho \right)^T \left(\frac{d\mu}{\mu} \right) + \left(K_\rho^c \Big|_\mu \right)^T \left(\frac{d\rho}{\rho} \right), \quad (15)$$

where the sensitivity kernels $K_\mu^c \Big|_\rho$ and $K_\rho^c \Big|_\mu$ are given by

$$K_{\mu,i}^c \Big|_\rho := \frac{1}{2k u v^T M v} \left[\mu_i v^T \frac{\partial (k^2 B_2 + B_0)}{\partial \mu_i} v \right], \quad (16)$$

$$K_{\rho,i}^c \Big|_\mu := \frac{-\omega}{2k u v^T M v} \left[\rho_i v^T \frac{\partial M}{\partial \rho_i} v \right]. \quad (17)$$

Here the subscript i in $K_{\mu,i}^c \Big|_\rho$ and $K_{\rho,i}^c \Big|_\mu$ denotes the i -th component of each sensitivity kernel (or gradient). Note that no summation is implied by the repeated indices i on the right-hand sides of equations 16 and 17. Moreover the familiar notation $\Big|_{\rho,\mu}$ indicates the parameter that is held constant.

Instead of using μ and ρ as the medium parameters, we can also choose the shear-wave velocity β and ρ . Since in an isotropic medium we have $\beta = \sqrt{\mu/\rho}$ it follows that to first order

$$\frac{d\mu}{\mu} = 2 \frac{d\beta}{\beta} + \frac{d\rho}{\rho}. \quad (18)$$

Using this in equation 15 it follows that we have

$$\frac{dc}{c} = \left(K_\beta^c \Big|_\rho \right)^T \left(\frac{d\beta}{\beta} \right) + \left(K_\rho^c \Big|_\beta \right)^T \left(\frac{d\rho}{\rho} \right), \quad (19)$$

where the sensitivity kernels $K_\mu^c \Big|_\beta$ and $K_\rho^c \Big|_\beta$ are given by

$$K_\beta^c \Big|_\rho := 2 K_\mu^c \Big|_\rho \quad \text{and} \quad K_\rho^c \Big|_\beta := K_\mu^c \Big|_\rho + K_\rho^c \Big|_\mu. \quad (20)$$

GROUP-VELOCITY INVERSION

Once the sensitivity kernels for the phase-velocity are known, the group-velocity sensitivity kernels can be derived from their phase-velocity equivalents. In general, the group velocity is related to the phase-velocity as

$$u = \frac{c}{1 - \frac{\omega}{c} \frac{\partial c}{\partial \omega}}. \quad (21)$$

Taking the logarithm on both side of this equation and introducing the notation $\tilde{u} := \log u$ and $\tilde{c} := \log c$ we get

$$\tilde{u} = \tilde{c} - \log \left(1 - \omega \frac{\partial \tilde{c}}{\partial \omega} \right). \quad (22)$$

Defining the model parameter vector $m = (\beta, \rho)^T$ and calculating the derivative of \tilde{u} with respect to $\tilde{m} = \log m$ we find [see also Rodi *et al.* (1975)]

$$\frac{\partial \tilde{u}}{\partial \tilde{m}} = \frac{\partial \tilde{c}}{\partial \tilde{m}} + \frac{u \omega}{c} \frac{\partial}{\partial \omega} \left(\frac{\partial \tilde{c}}{\partial \tilde{m}} \right). \quad (23)$$

Writing it out explicitly in terms of u and c and medium parameters β and ρ we get

$$\frac{du}{u} = \frac{dc}{c} + \frac{u \omega}{c} \frac{\partial}{\partial \omega} \left(\frac{\beta}{c} \frac{\partial c}{\partial \beta} \right) \frac{d\beta}{\beta} + \frac{u \omega}{c} \frac{\partial}{\partial \omega} \left(\frac{\rho}{c} \frac{\partial c}{\partial \rho} \right) \frac{d\rho}{\rho}. \quad (24)$$

Knowing that by definition of the sensitivity kernels $K_\beta^c \Big|_\rho$ and $K_\rho^c \Big|_\beta$ we have

$$K_\beta^c \Big|_\rho = \frac{\beta}{c} \frac{\partial c}{\partial \beta}, \quad \text{and} \quad K_\rho^c \Big|_\beta = \frac{\rho}{c} \frac{\partial c}{\partial \rho}, \quad (25)$$

it follows that

$$\frac{du}{u} = \left(K_\beta^u \Big|_\rho \right)^T \left(\frac{d\beta}{\beta} \right) + \left(K_\rho^u \Big|_\beta \right)^T \left(\frac{d\rho}{\rho} \right), \quad (26)$$

with the group-velocity sensitivity kernels $K_\beta^u \Big|_\rho$ and $K_\rho^u \Big|_\beta$ given by

$$K_\beta^u \Big|_\rho := K_\beta^c \Big|_\rho + \frac{u \omega}{c} \frac{\partial K_\beta^c \Big|_\rho}{\partial \omega}, \quad (27)$$

$$K_\rho^u \Big|_\beta := K_\rho^c \Big|_\beta + \frac{u \omega}{c} \frac{\partial K_\rho^c \Big|_\beta}{\partial \omega}. \quad (28)$$

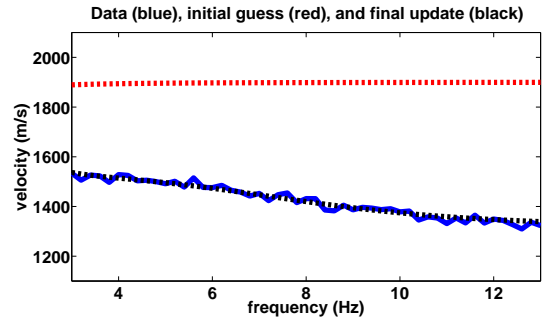


Figure 2: Data space for an example of Love wave group velocity inversion. Shown are the initial data (red), the synthetic data corrupted by 1% Gaussian noise (blue), and the data from the final inversion result (black).

In Figures 2 and 3 we show an example of group velocity inversion of the fundamental mode for a model with a low velocity layer at depth. The inversion is implemented using a damped least-squares scheme. Though we take a homogeneous model as the initial guess, a smooth version of the low velocity layer is recovered in the final inversion result as shown in Figure 3. It is remarkable that the inversion is able to converge to an acceptable solution considering that Love waves, strictly

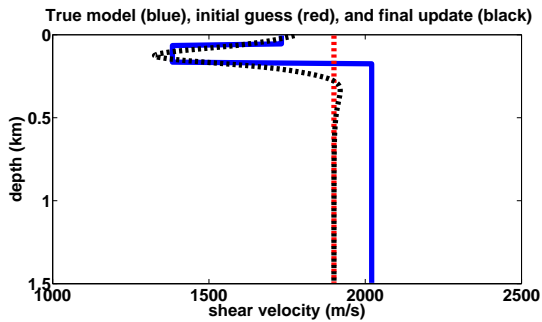


Figure 3: Model space for an example of Love wave group velocity inversion. Shown are the initial model (red), the true model used to generate the synthetic data, and the final inverted model (black).

speaking, do not exist in an initial homogeneous model. We are currently investigating how the existence of Love waves in the initial model affects the performance of the inversion algorithm.

INVERSION OF SHEAR STRESS RATIO

In Aki & Richards (2002) equation 7.20, the phase of the two shear stresses in the SH-system, τ_{xy} and τ_{yz} , differ by a factor of the imaginary number i . Thus, the two shear stresses execute an analogy of elliptical motion. Since we know that the ellipticity of Rayleigh waves can be inverted for shear velocity structure (Tanimoto & Tsuboi, 2009; Haney *et al.*, 2011), we find that the ratio of these two shear stress components is also sensitive to structure and has the potential to be inverted. Thus, we can extend the concept of HZ ratio inversion used in analyzing Rayleigh waves to Love waves.

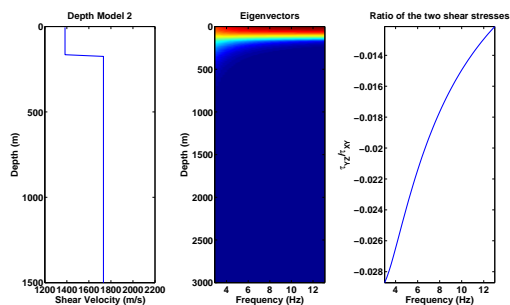


Figure 4: A model with a low velocity layer at the surface is shown in the left panel. In the middle and right panels, we plot the eigenvectors for this model and the ratio of the shear stresses as a function of frequency.

Note that the shear stress ratio goes to zero at the surface, $z = 0$, since the yz -component of the shear stress goes to zero at the free surface by definition. Thus, to measure this quantity in practice requires that geophones be buried at some depth below the surface. In principle, the ratio requires that τ_{xy} and τ_{yz} be measured, which presents some difficulty. From Aki &

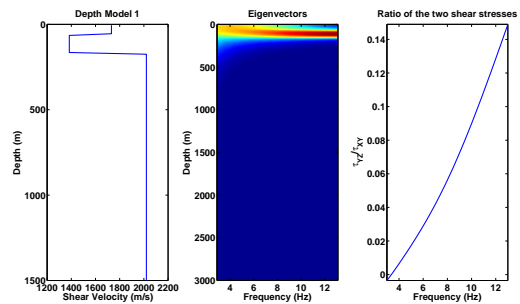


Figure 5: A model with a low velocity layer at depth is shown in the left panel. In the middle and right panels, we plot the eigenvectors for this model and the ratio of the shear stresses as a function of frequency.

Richards (2002), we know that τ_{xy} and τ_{yz} can generally be expressed as

$$\tau_{yz} = \mu \frac{dL}{dz} \quad (29)$$

and

$$\tau_{xy} = i\mu L \frac{\omega}{c} \quad (30)$$

where L is the mode shape of the Love wave eigenfunction and μ is the shear modulus. Although one would need to know μ to measure the shear stresses, this quantity cancels when taking their ratio. Thus, the measurement of τ_{yz}/τ_{xy} in practice simply requires that vertical and horizontal derivatives of the wavefield be measured. Such measurements can be made by placing two geophones close to each other in the horizontal or vertical direction and taking finite-differences between the.

In Figures 4 and 5, we show the ratio of the shear stresses for two different models using synthetic forward modeled data generated with the method described earlier. The ratio is calculated at a depth of 10 m. As seen in the two figures, the ratio changes significantly between the models, showing that it is sensitive to depth structure. In the future, we plan to invert these curves of the shear stress ratio as a function of frequency for shear velocity profiles. In addition, we will consider ratios of stresses associated with the P-SV system in the future for Rayleigh waves.

CONCLUSION

We have presented the theory of one-dimensional Love wave inversion using phase velocity, group velocity, and shear stress ratio measurements. This theory can be used for practical inversion of such measurements.

ACKNOWLEDGEMENTS

We thank ION Geophysical/GXT Imaging solutions for permission to publish these results.

REFERENCES

- Aki, K., and Richards, P. G., 2002, Quantitative seismology: , University Science Books, Sausalito, California, 2nd edition.
- Dorman, J., and Ewing, M., 1962, Numerical inversion of seismic surface wave dispersion data and crust-mantle structure in the new york-pennsylvania area: *Geophysics*, **67**, 5227–5241.
- Gouédard, P., Yao, H., van der Hilst, R., and Verdel, A., 2010, Surface-wave eikonal tomography in a scattering environment: Expanded abstracts of the SEG Annual Meeting.
- Haney, M. M., Nies, A., Masterlark, T., Needy, S., and Pedersen, R., 2011, Interpretation of rayleigh-wave ellipticity observed with multicomponent passive seismic interferometry at hekla volcano, iceland: *The Leading Edge*, **30**, 936–941.
- Ivanov, J., Miller, R., Lacombe, P., Johnson, C., and Lane Jr., J., 2006, Delineating a shallow fault zone and dipping bedrock strata using multichannel analysis of surface waves with a land streamer: *Geophysics*, **71**, A39–A42.
- Kausel, E., and Roësset, J. M., 1981, Stiffness matrices for layered soils: *Bulletin of the Seismological Society of America*, **71**, 1743–1761.
- Komatitsch, D., and Vilotte, J. P., 1998, The spectral-element method: an efficient tool to simulate the seismic response of 2D and 3D geological structures: *Bull. Seis. Soc. Am*, **88**, no. 2, 368–392.
- Lysmer, J., and Drake, L., 1971, The propagation of love waves across nonhorizontally layered structures: *Bull. Seis. Soc. Am*, **61**, no. 5, 1233–1251.
- Lysmer, J., 1970, Lumped mass method for rayleigh waves: *Bull. Seis. Soc. Am*, **60**, no. 1, 89–104.
- Masterlark, T., Haney, M., Dickinson, H., Fournier, T., and Searcy, C., 2010, Rheologic and structural controls on the deformation of okmok volcano, alaska: Fems, insar, and ambient noise tomography: *Journal of Geophysical Research*, **115**, B02409.
- Muyzert, E., 2007, Seabed property estimation from ambient-noise recordings: Part 2 - scholte-wave spectral-ratio inversion: *Geophysics*, **74**, U47–U53.
- Nolet, G., Sleeman, R., Nijhof, V., and Kennett, B. L. N., 1989, Synthetic reflection seismograms in three dimensions by a locked-mode approximation: *Geophysics*, **54**, 350–358.
- Patera, A. T., 1984, A spectral element method for fluid dynamics: laminar flow in a channel expansion: *Journal of Computational Physics*, **54**, 468–488.
- Rodi, W. L., Glover, P., Li, T. M. C., and Alexander, S. S., 1975, A fast, accurate method for computing group-velocity partial derivatives for rayleigh and love modes: *Bull. Seis. Soc. Am*, **65**, 1105–1114.
- Tanimoto, T., and Tsuboi, S., 2009, Variational principle for rayleigh wave ellipticity: *Geophysical Journal International*, **179**, 1658–1668.
- Xia, J., Miller, R., and Park, C., 1999, Estimation of near-surface shear-wave velocity by inversion of rayleigh waves: *Geophysics*, **64**, 691–700.